Local skewness attribute as a seismic phase detector[a]

[a]Published in Interpretation, 2, no. 1, SA49-SA56, (2014)

Sergey Fomel[*] *and Mirko van der Baan*[†]

ABSTRACT

We propose a novel seismic attribute, local skewness, as an indicator of localized phase of seismic signals. The proposed attribute appears to have a higher dynamical range and a better stability than the previously used local kurtosis. Synthetic and real data examples demonstrate the effectiveness of local skewness in detecting and correcting time-varying, locally-observed phase of seismic signals.

INTRODUCTION

Wavelet phase is an important characteristic of seismic signals. Physical causal systems exhibit minimum-phase behavior (Robinson and Treitel, 2000). For purposes of seismic interpretation, it is convenient to deal with zero-phase wavelets with minimum or maximum amplitudes centered at the horizons of interest because it leads to the highest resolution as well as more accurate estimates of both reflection times and spacings (Schoenberger, 1974). Zero-phase correction is therefore a routine procedure applied to seismic images before they are passed to the interpreter (Brown, 1999).

It is important to make a distinction between phases of *propagating* and *locally observed* wavelets (Van der Baan et al., 2010b,a). The former is the physical wavelet that propagates through the Earth, thereby sampling the local geology. It is subject to geometric spreading, attenuation, and concomitant dispersion. The latter is the wavelet as observed at a certain point in space and time. Its immediate shape results from its interaction (convolution) with the reflectivity of the Earth and the current shape of the propagating wavelet. For instance, a thin layer with a positive change in seismic impedance has opposite polarities of seismic reflectivities at the top and the bottom interface, which make it act like a derivative filter and generate a wavelet with the locally observed phase subjected to a 90° rotation (Zeng and Backus, 2005). In the absence of well log information, it is usually difficult to separate unambiguously the locally observed phase from the phase of the propagating wavelet. Nevertheless, measuring the local phase can provide a useful attribute for analyzing seismic data (Van der Baan and Fomel, 2009; Fomel and van der Baan, 2010; Van der Baan et al., 2010a; Xu et al., 2012).

Levy and Oldenburg (1987) proposed a method of phase detection based on maximization of the varimax norm or kurtosis as an objective measure of zero-phaseness. By rotating the phase and measuring the kurtosis of seismic signals, one can detect the phase rotations necessary for zero-phase correction (Van der Baan, 2008). Van der Baan and Fomel (2009) applied local kurtosis, a smoothly nonstationary measure (Fomel et al., 2007), and demonstrated its advantages in measuring phase variations as compared with kurtosis measurements in sliding windows. Local kurtosis is an example of a local attribute (Fomel, 2007a) defined by utilizing regularized least-squares inversion.

In this paper, we revisit the problem of phase estimation and propose a novel attribute, *local skewness*, as a phase detector. Analogous to local kurtosis, local skewness is defined using local similarity measurements via regularized least squares. This attribute is maximized when the locally observed phase is close to zero. Advantages of the new attribute are a higher dynamical range and a better stability, which make it suitable for picking phase corrections. Using synthetic and field-data examples, we demonstrate properties and applications of the proposed attribute.

LOCALIZED PHASE ESTIMATION

Our goal is to estimate the time-variant, localized phase from seismic data. What objective measure can indicate that a certain signal has a zero phase? One classic measure is the varimax norm or kurtosis (Wiggins, 1978; Levy and Oldenburg, 1987; White, 1988). Varimax is defined as

$$\phi[\mathbf{s}] = \frac{N \sum_{n=1}^{N} s_n^4}{\left(\sum_{n=1}^{N} s_n^2 \right)^2} , \tag{1}$$

where $\mathbf{s} = \{s_1, s_2, \ldots, s_N\}$ represents a vector of seismic amplitudes inside a window of size N. Varimax is simply related to kurtosis of zero-mean signals.

The statistical rationale behind the Wiggins algorithm and its variants is that convolution of any filter with a time series that is white with respect to all statistical orders makes the outcome more Gaussian. The optimum deconvolution filter is therefore one that ensures the deconvolution output is maximally non-Gaussian (Donoho, 1981). The constant-phase assumption made by Levy and Oldenburg (1987) and White (1988) reduces the number of free parameters to one, thereby stabilizing performance compared with the Wiggins method. Wavelets derived in seismic-to-well ties often have a near-constant phase, thus justifying this assumption.

Noticing that the correlation coefficient of two sequences a_n and b_n is defined as

$$\gamma[\mathbf{a},\mathbf{b}] = \frac{\sum_{n=1}^{N} a_n\, b_n}{\sqrt{\sum_{n=1}^{N} a_n^2 \sum_{n=1}^{N} b_n^2}} \tag{2}$$

and the correlation of a_n with a constant is

$$\gamma[\mathbf{a},\mathbf{1}] = \frac{\sum_{n=1}^{N} a_n}{\sqrt{N \sum_{n=1}^{N} a_n^2}}\ , \tag{3}$$

Fomel et al. (2007) interpreted the kurtosis measure in equation 1 as the inverse of the squared correlation coefficient between s_n^2 and a constant, $\phi[\mathbf{s}] = 1/\gamma^2[\mathbf{s}^2,\mathbf{1}]$. Well-focused or zero-phase signals exhibit low correlation with a constant and correspondingly higher kurtosis (Figure 1). This provides an alternative interpretation to the goal of making the deconvolution outcome maximally non-Gaussian for desired phase estimation. Note that equation 2 is usually applied to zero-mean sequences **a** and **b**. This is neglected in the derivation of expression 3.

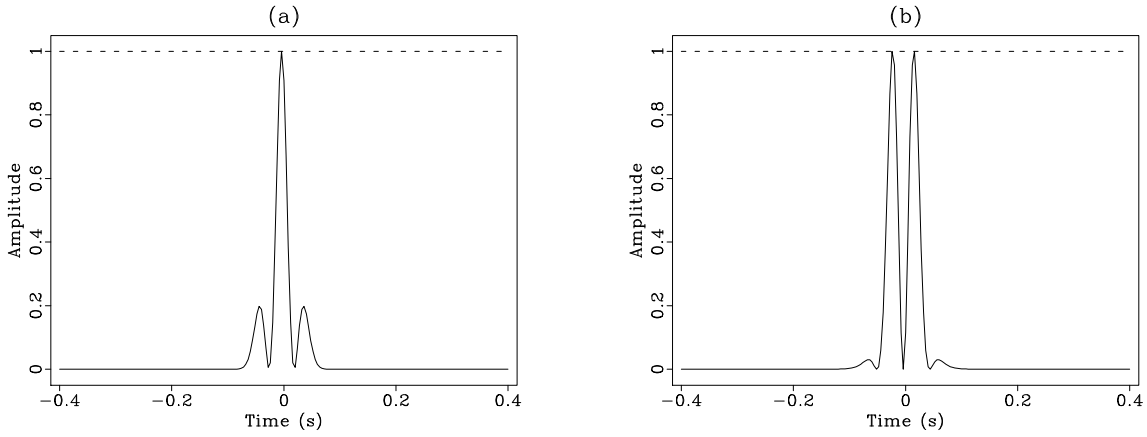

Figure 1: (a) Squared 0°-phase Ricker wavelet compared with a constant. (b) Squared 90°-phase Ricker wavelet compared with a constant. The 90°-phase signal has a higher correlation with a constant and correspondingly a lower kurtosis.

In this paper, we suggest a different measure, skewness, for measuring the apparent phase of seismic signals. Skewness of a sequence s_n is defined as (Bulmer, 1979)

$$\kappa[\mathbf{s}] = \frac{\frac{1}{N}\sum_{n=1}^{N} s_n^3}{\left(\frac{1}{N}\sum_{n=1}^{N} s_n^2\right)^{3/2}}\ . \tag{4}$$

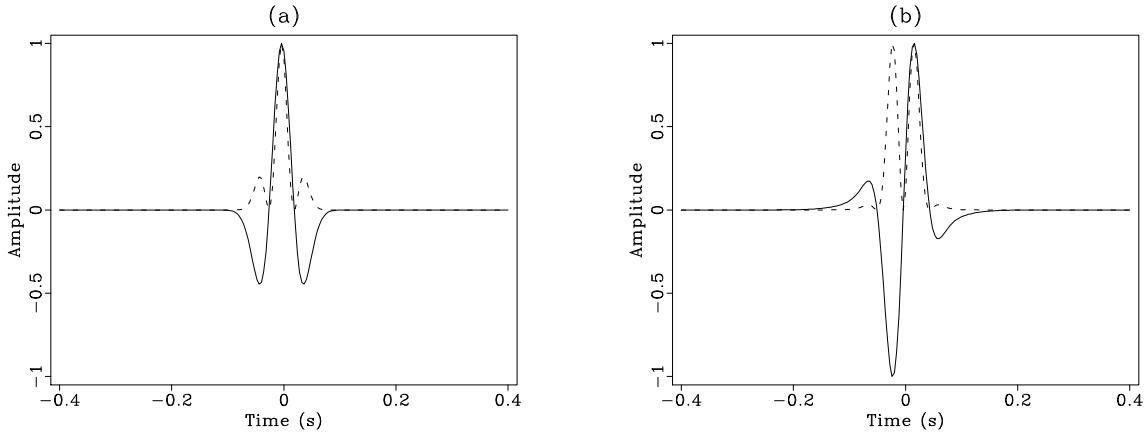

Figure 2: (a) 0°-phase Ricker wavelet compared with its square. (b) 90°-phase Ricker wavelet compared with its square. The 0°-phase has a stronger correlation with its square and correspondingly a higher skewness.

In statistics, skewness is used for measuring asymmetry of probability distributions. Simple algebraic manipulations show that skewness squared can be represented as

$$\kappa^2[\mathbf{s}] = \frac{\left(\sum_{n=1}^{N} s_n^2 \cdot s_n\right)^2}{\sum_{n=1}^{N} s_n^4 \sum_{n=1}^{N} s_n^2} \frac{\sum_{n=1}^{N} s_n^4 \sum_{n=1}^{N} 1^2}{\left(\sum_{n=1}^{N} s_n^2\right)^2} = \frac{\gamma^2[\mathbf{s}^2, \mathbf{s}]}{\gamma^2[\mathbf{s}^2, \mathbf{1}]} = \phi[\mathbf{s}]\, \gamma^2[\mathbf{s}^2, \mathbf{s}] \; . \tag{5}$$

In other words, squared skewness is equal to the kurtosis measure modulated by the squared correlation coefficient between the signal and its square. Zero-phase signals tend to exhibit higher correlation with the square and correspondingly higher skewness (Figure 2). Following experiments with synthetic and field data, we find it advantageous to use sometimes the inverse skewness

$$\frac{1}{\kappa^2[\mathbf{s}]} = \frac{\gamma^2[\mathbf{s}^2, \mathbf{1}]}{\gamma^2[\mathbf{s}^2, \mathbf{s}]} \; . \tag{6}$$

Unlike kurtosis which measures non-Gaussianity, skewness is related to asymmetry. Whereas convolution of two non-Gaussian sequences makes the outcome more Gaussian, convolution of two asymmetric series becomes more symmetric. Both phenomena are a consequence of the central limit theorem. A zero-phase wavelet is more compact than a nonzero phase one (Schoenberger, 1974), and therefore also more asymmetric. Skewness-based criteria can thus detect the appropriate wavelet phase by applying a series of constant phase rotations to the data and then evaluating the angle that produces the most skewed distribution.

The two measures do not necessarily agree with one another, which is illustrated in Figures 3 and 4. For an isolated positive spike convolved with a compact zero-phase

wavelet, the two measures agree in the picking of the zero-phase result as having both a high kurtosis and a high skewness (Figure 3). For a slightly more complex case of a double positive spike convolved with the same wavelet (Figure 4), the two measures disagree: kurtosis picks a signal rotated by 90° whereas skewness picks the original signal. Note that, in both examples, skewness exhibits a significantly higher dynamical range, which makes it more suitable for picking optimal phase rotations.

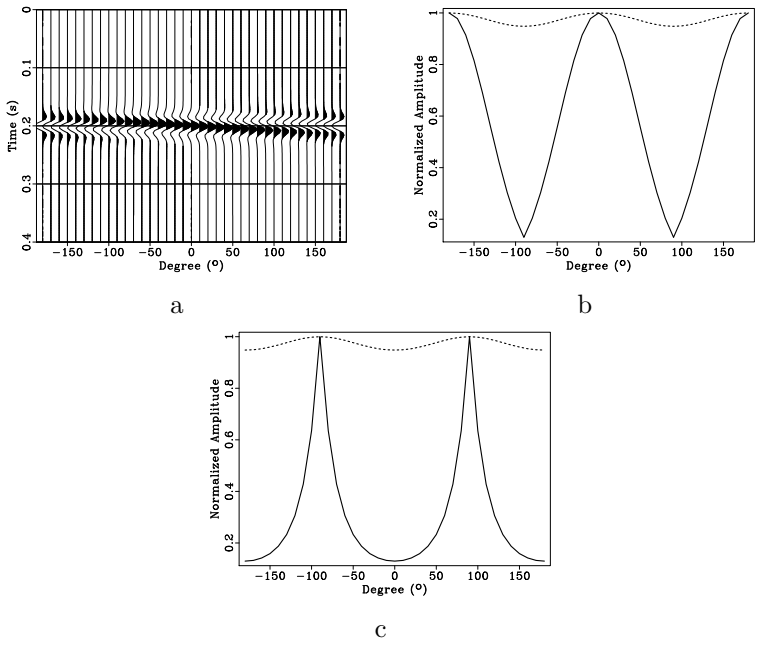

a b c

Figure 3: (a) Ricker wavelet rotated through different phases. (b) Skewness (solid line) and kurtosis (dashed line) as functions of the phase rotation angle. (c) Inverse skewness (solid line) and inverse kurtosis (dashed line) as functions of the phase rotation angle. The two measures agree in picking the signal at 0° and 180°. Note the higher dynamical range of skewness.

DEFINING SKEWNESS AS A LOCAL ATTRIBUTE

The method of local attributes (Fomel, 2007a) is a technique for extending stationary or instantaneous attributes to smoothly varying or nonstationary attributes by employing a regularized least-squares formulation. In particular, the scalar correlation coefficient γ in equation 2 is replaced with a vector, $\mathbf{c}$, defined as a componentwise product of vectors $\mathbf{c}_1$ and $\mathbf{c}_2$, where

$$\mathbf{c}_1 = \left[\lambda^2 \mathbf{I} + \mathbf{S}\left(\mathbf{A}^T\mathbf{A} - \lambda^2\mathbf{I}\right)\right]^{-1} \mathbf{S}\,\mathbf{A}^T\mathbf{b}\,, \tag{7}$$

$$\mathbf{c}_2 = \left[\lambda^2 \mathbf{I} + \mathbf{S}\left(\mathbf{B}^T\mathbf{B} - \lambda^2\mathbf{I}\right)\right]^{-1} \mathbf{S}\,\mathbf{B}^T\mathbf{a}\,. \tag{8}$$

In equations 7-8, $\mathbf{a}$ and $\mathbf{b}$ are vectors composed of a_n and b_n, respectively; $\mathbf{A}$ and $\mathbf{B}$ are diagonal matrices composed of the same elements; and $\mathbf{S}$ is a smoothing operator.

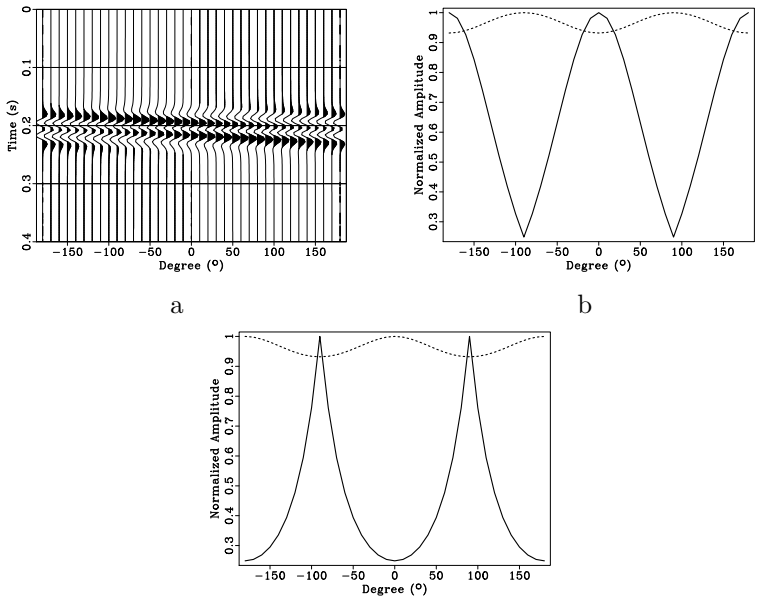

a b c

Figure 4: (a) Ricker wavelet convolved with a double impulse and rotated through different phases. (b) Skewness (solid line) and kurtosis (dashed line) as functions of the phase rotation angle. (c) Inverse skewness (solid line) and inverse kurtosis (dashed line) as functions of the phase rotation angle. The two measures disagree by 90° in picking the optimal phase. The skewness attribute picks a better focused signal.

We use triangle smoothing (Claerbout, 1992) controlled by specifying the smoothing radius, which can be different in vertical and horizontal directions.

Regularized inversion appearing in equations 7 and 8 is justified in the method of shaping regularization (Fomel, 2007b). The corresponding local similarity attribute has been used previously to align multicomponent and time-lapse images (Fomel, 2007a; Fomel and Jin, 2009; Kazemeini et al., 2010; Zhang et al., 2013), to detect focusing of diffractions (Fomel et al., 2007), to enhance stacking (Liu et al., 2011a, 2009), to create time-frequency distributions (Liu et al., 2011b), and to perform zero-phase correction with local kurtosis (Van der Baan and Fomel, 2009). In this paper, we apply it to zero-phasing seismic data using local skewness.

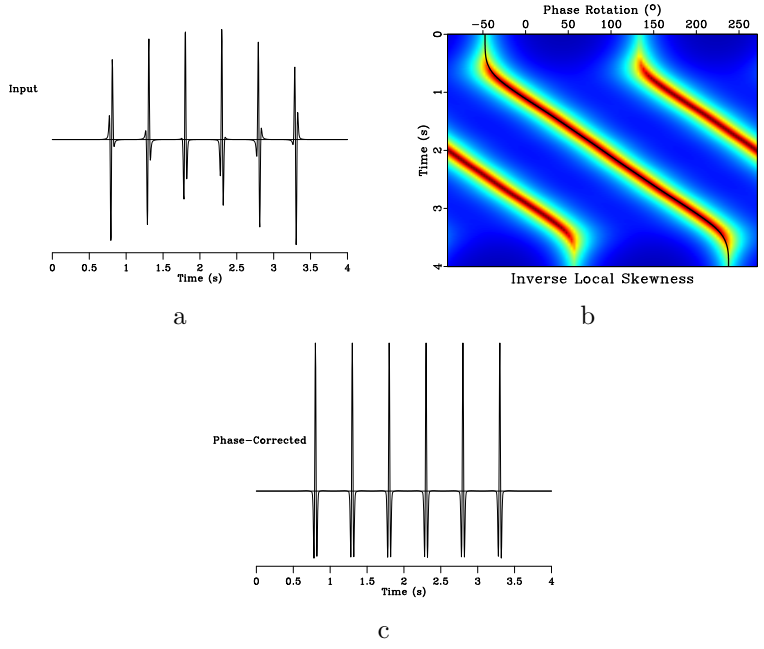

Figure 5: (a) Input synthetic trace with variable-phase events. (b) Inverse local skewness as a function of the phase rotation angle. Red colors correspond to high inverse similarity. (c) Synthetic trace after non-stationary rotation to zero phase using picked phase.

We illustrate the proposed zero-phase correction procedure in Figure 5. The input synthetic trace contains a set of Ricker wavelets with a gradually variable phase (Figure 5a). We start with a number of phase rotations with different angles, each time computing the local skewness. The result of this step is displayed in Figure 5b and shows a clear high-similarity trend. After picking the trend, adding 90° to it, and performing the corresponding nonstationary trace rotation, we end up with the phase-corrected trace, shown in Figure 5c. All the original phase rotations are clearly detected and removed. The radius of the regularization smoothing in this example was 100 samples or 0.4 s.

APPLICATION EXAMPLE

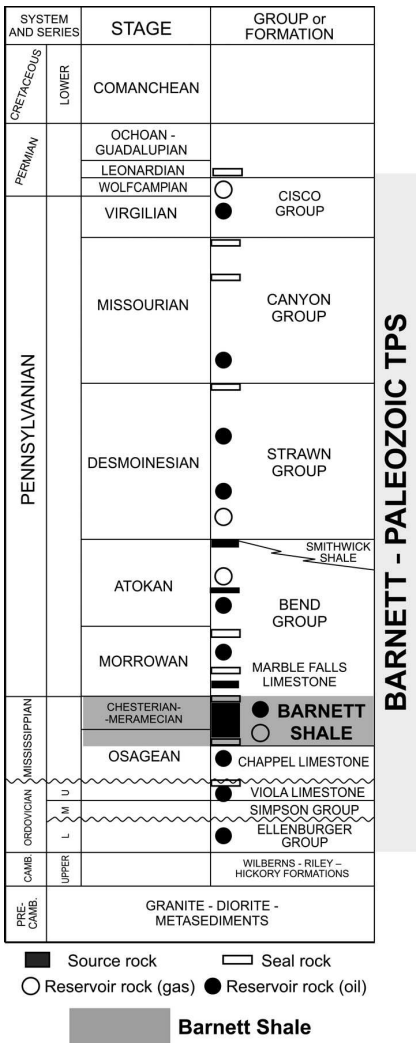

Figure 6: Stratigraphic column of the Fort Worth Basin where the Boonsville dataset is located, after Pollastro et al. (2007). Karstification in the Ellenburger Carbonates has caused local sags in the overlying Barnett and Bend Conglomerate formations, creating reservoir compartmentalization.

.

The input dataset for our field-data example is the Boonsville dataset from the Fort Worth Basin in North-Central Texas, USA (Hardage et al., 1996a,b). The formations of interest are the Ellenburger Carbonates, the Barnett Shale and the Bend Conglomerates (see Figure 6 for a stratigraphic column). The Ellenburger Carbonates are of Ordovician age. Their karstification due to post-Ellenburger carbonate dissolution and subsequent cavern collapses has created sags in the overlying formations, affecting sedimentation patterns and structures in the overlying Barnett Shales and Bend Conglomerates. The collapse features look like vertical chimneys with roughly

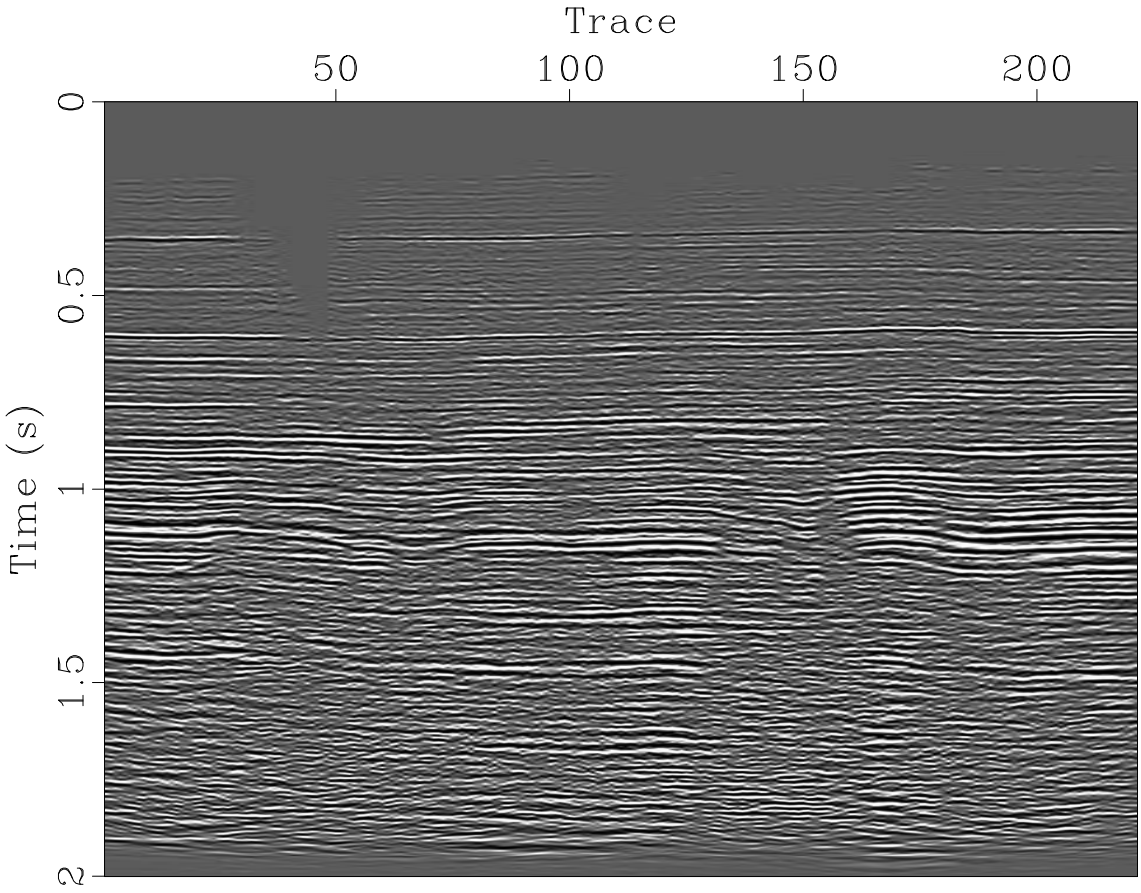

Figure 7: Input data: a section of the Boonsville dataset

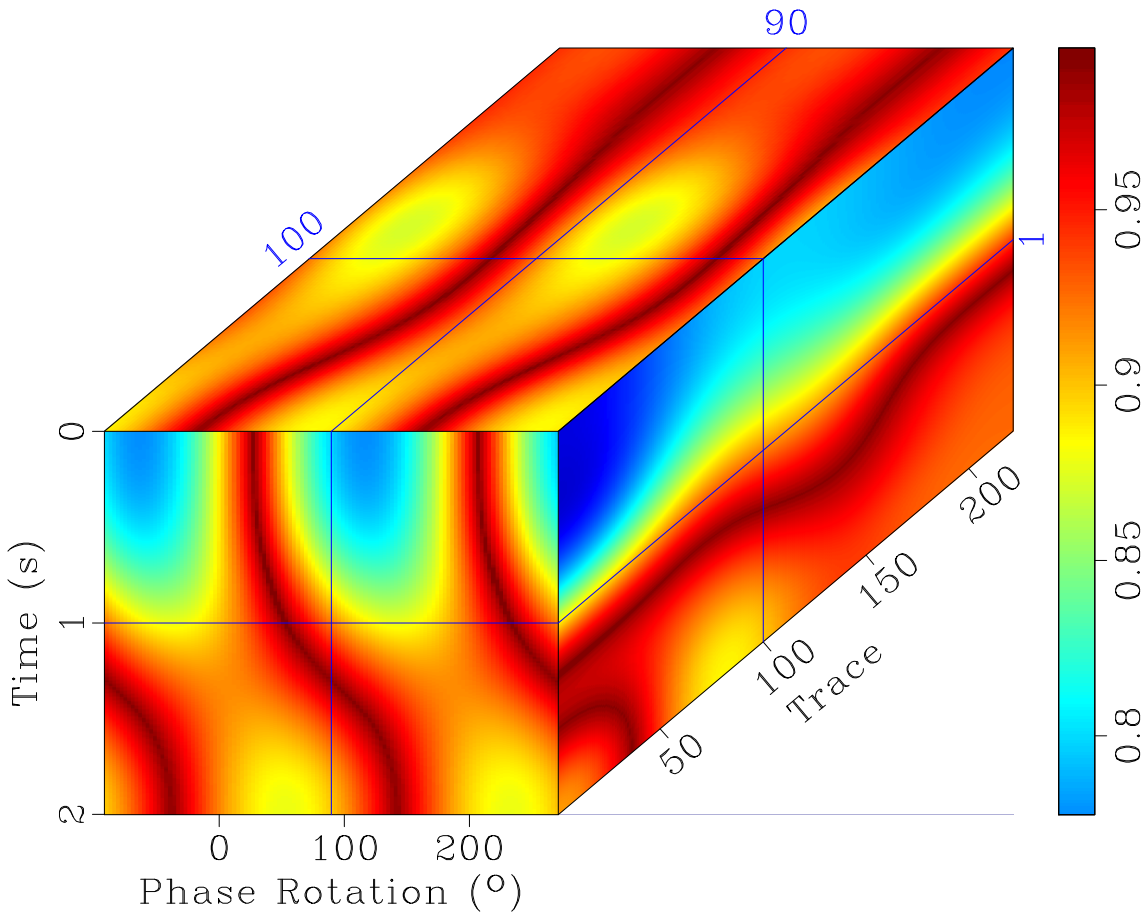

Figure 8: Inverse local skewness as a function of the phase rotation angle, with application to the section from Figure 7. Red colors correspond to high inverse similarity.

circular cross-sections, extending up to 600-760 m above the Ellenburger Carbonates (Hardage et al., 1996a), sometimes even reaching into the Strawn Group above the Bend Conglomerates.

The Barnett Shales are of Mississippian age. They are the target of much current exploitation in Texas as these are tight-shale reservoirs (Pollastro et al., 2007). Zones with karst-induced cavern collapses form a drilling and completion hazard for the mainly horizontal drilling programs in these tight-shale reservoirs and must be mapped. They may affect local fracture densities and thus permeabilities and reservoir drainage positively but can also lead to fluid barriers due to reservoir compartmentalization.

The shallower clastic Bend Conglomerates are of Middle Pennsylvanian (Atokan) age. The formation has a thickness of 300-360 m in this area with depths between 1370 to 1830 m. It was targeted throughout the 1980s and 1990s as it contains several gas and oil-bearing reservoirs in a stacked fashion. Hardage et al. (1996a,b) describe how the karstification has greatly impacted the system tracts and sedimentation patterns in the Bend formation which were characterized by low accommodation space. Resulting reservoir compartmentalization is a significant challenge for this formation and has also affected the reflector character. Reflection near the base of this formation display both reflector weakening and sometimes even polarity reversals in areas depressed due to local sagging. Acquisition and processing of this dataset are described by Hardage et al. (1996a). A stacked section is shown in Figure 7. A zero-phase correction has been applied to the data but has left regions with variable localized phase.

Our processing sequence is similar to the one used in Figure 5. First, we apply a number of phase rotations with different angles and compute local skewness for each rotation. The regularization lengths in this examples were 500 samples or 0.5 s in time and 50 traces in space. The result is displayed in Figure 8. Next, we apply automatic picking with the algorithm described by Fomel (2009) to extract the nonstationary phase rotation that maximizes the local skewness. Finally, the phase correction is applied to the data, with the result displayed in Figure 9. A zoomed-in comparison shows the effects of non-stationary phase correction: rotating major seismic events to zero degrees and improving their continuity. These effects can be useful both for improving structural interpretation and for improved matching of seismic data and well logs.

We applied the local phase detection to the 3-D volume in a window centered on the target horizon (Figure 10). The estimated local phase variation along the target horizon is shown in Figure 11. Comparing the amplitude before and after phase correction (Figure 12), we observe a noticeable improvement in event continuity. Once the processing and interpretation are done on the zero-phase-corrected volume, it is easy to restore the original phase by applying the inverse phase rotation.

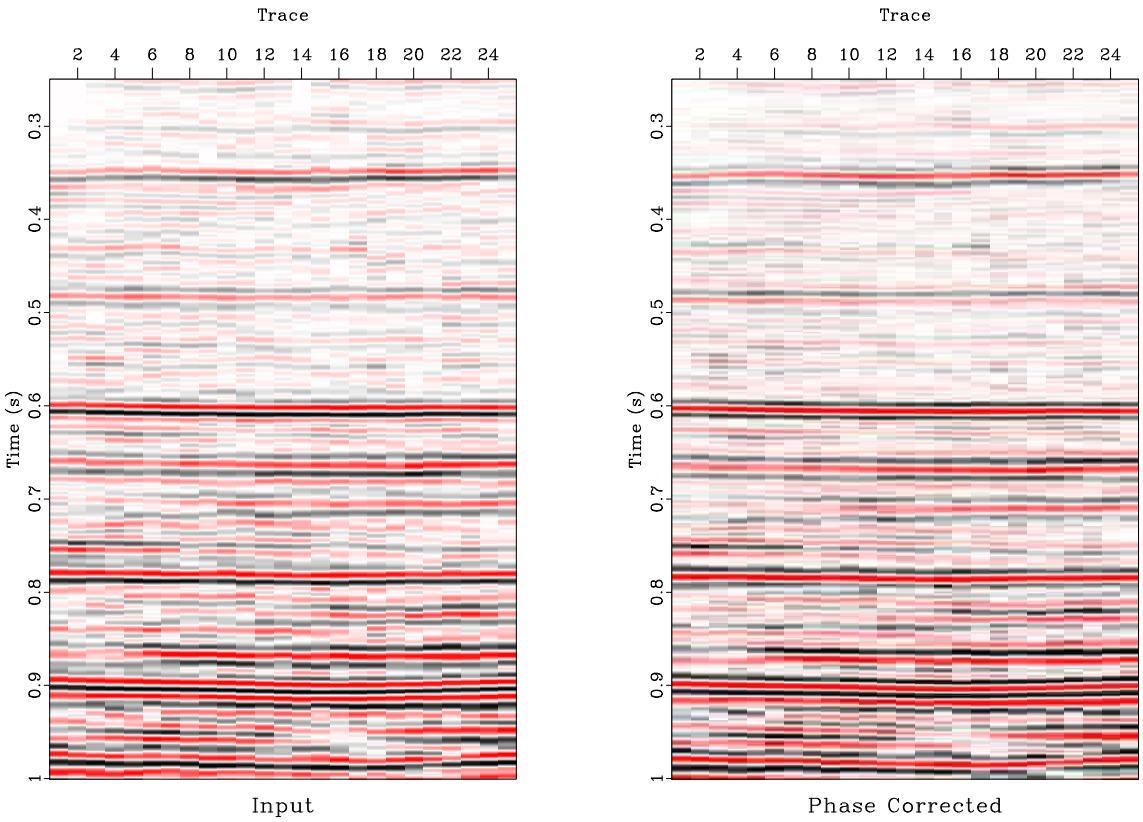

Figure 9: Zoomed-in comparison of the data before phase correction (a) and after phase correction (b). Nonstationary phase correction helps in identifying significant horizons and increasing their resolution in time.

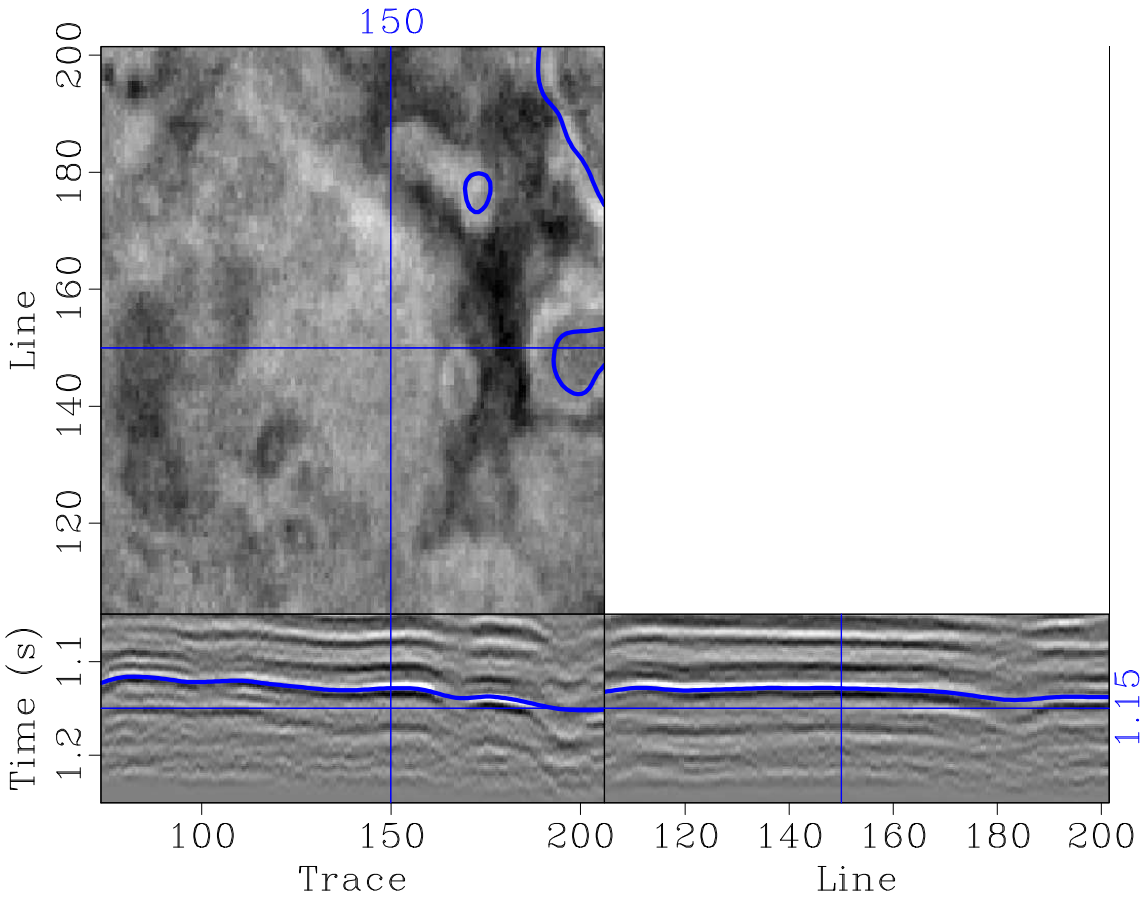

Figure 10: Boonsville dataset windowed around the target horizon.

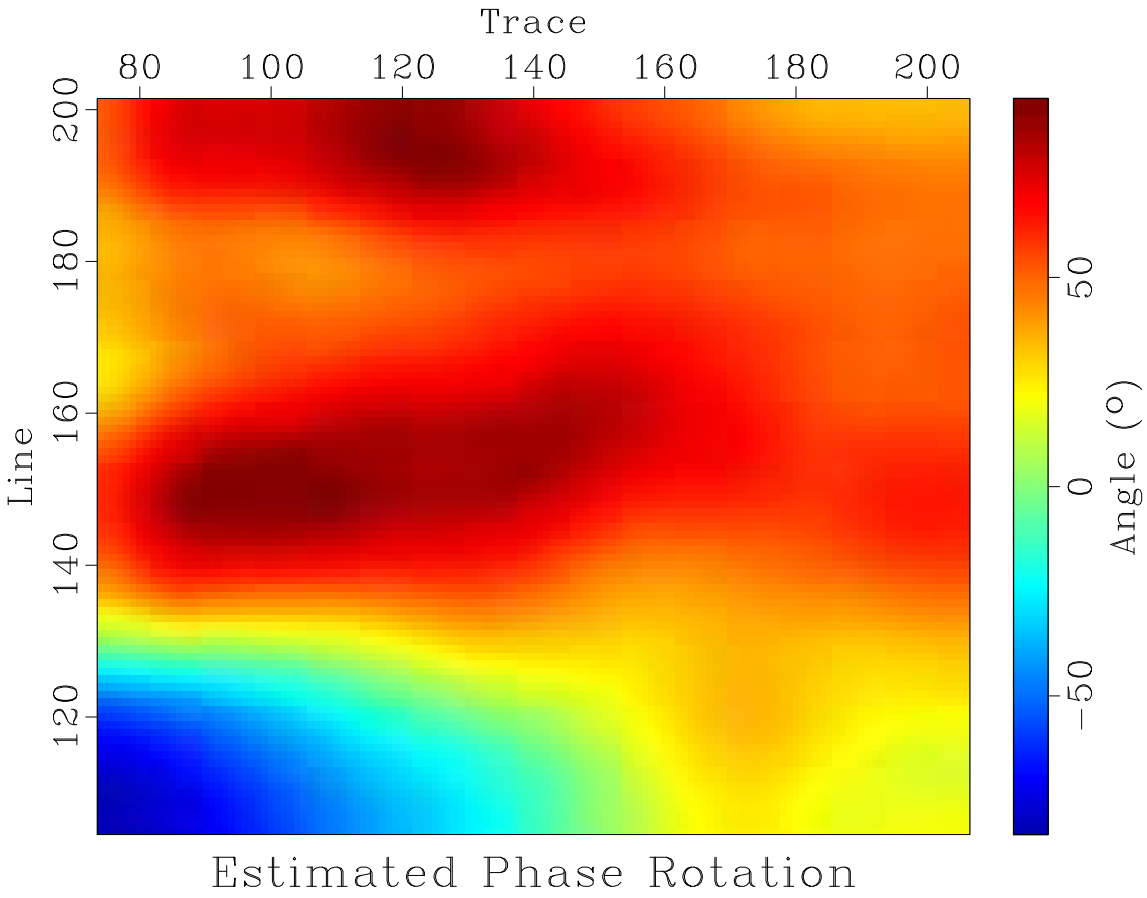

Figure 11: Local phase variation along the target horizon estimated from the data shown in Figure 10.

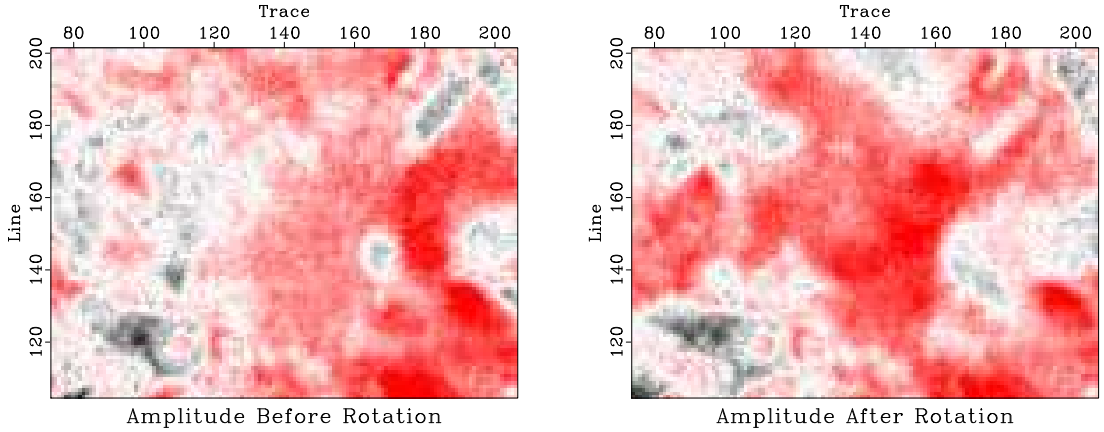

a b

Figure 12: Amplitude along the target horizon before and after phase rotation.

DISCUSSION

The data example as well as the previous case studies by Van der Baan et al. (2010b) underline how analysis of the local phase can be used as a complementary attribute to spectral decomposition to highlight variations in wavelet character. There are two complimentary applications, namely analysis of the propagating and locally observed wavelets. The targeted wavelet type is determined by the chosen regularization length: the propagating wavelet is estimated by using long temporal regularization lengths, and the locally observed one from shorter lengths. The underlying assumption is that, for long regularization lengths, variations in the local geology are averaged out, revealing only the propagating wavelet. In this paper, we used relatively short regularization lengths as the aim is to highlight changes in the local reflection character.

Well-log analyses have demonstrated that the Earth's reflectivity series is non-Gaussian (Walden and Hosken, 1986) and, to first order, white (Walden and Hosken, 1985). In addition, impedances tend to increase with depth, hence positive reflection coefficients are slightly more likely than negative one, producing an asymmetric reflectivity distribution. Statistically, the skewness-based criterion assumes that the Earth's reflectivity series are white and asymmetric. This is in contrast to kurtosis used previously by Van der Baan and Fomel (2009), which assumes a non-Gaussian reflectivity series. Both the non-Gaussianity and asymmetry assumptions seem warranted but may fail if the local reflectivity series becomes respectively purely Gaussian or symmetric.

The local skewness attribute has the advantage over kurtosis because of its higher dynamic range, which facilitates picking. Variance is the second statistical order, skewness is the third one, and kurtosis is related to the fourth order. Estimation variances increases with the order of a moment (Mendel, 1991). In other words, less samples are needed to estimate skewness with the same accuracy as kurtosis. We hypothesize that this contributes to the higher dynamic range of the skewness criterion.

CONCLUSIONS

We have presented a novel approach to nonstationary identification of apparent (locally observed) phase. Our approach is based on a new attribute, local skewness. In synthetic and field-data examples, local skewness exhibits a tendency to pick focused signals and a higher dynamical range than the previously used local kurtosis. Its computation involves a local similarity between the input signal and its square. Practical applications of using local skewness for zero-phase correction of seismic signals should be combined with well-log analysis in order to better separate the locally-observed phase from the propagating-wavelet phase.

ACKNOWLEDGMENTS

We thank Milo Backus, Guochang Liu, Mike Perz, and Hongliu Zeng for stimulating discussions.

REFERENCES

Brown, A. R., 1999, Interpretation of three-dimensional seismic data: AAPG and SEG.

Bulmer, M., 1979, Principles of statistics: Dover Publications.

Claerbout, J. F., 1992, Earth Soundings Analysis: Processing Versus Inversion: Blackwell Scientific Publications.

Donoho, D., 1981, On minimum entropy deconvolution, *in* Applied time series analysis II: Academic Press, 565–608.

Fomel, S., 2007a, Local seismic attributes: Geophysics, **72**, A29–A33.

———, 2007b, Shaping regularization in geophysical-estimation problems: Geophysics, **72**, R29–R36.

———, 2009, Velocity analysis using AB semblance: Geophysical Prospecting, **57**, 311–321.

Fomel, S., and L. Jin, 2009, Time-lapse image registration using the local similarity attribute: Geophysics, **74**, A7–A11.

Fomel, S., E. Landa, and M. T. Taner, 2007, Post-stack velocity analysis by separation and imaging of seismic diffractions: Geophysics, **72**, U89–U94.

Fomel, S., and M. van der Baan, 2010, Local similarity with the envelope as a seismic phase detector, *in* 80th Ann. Internat. Mtg: Soc. of Expl. Geophys., 1555–1559.

Hardage, B. A., D. L. Carr, D. E. Lancaster, J. L. Simmons Jr, R. Y. Elphick, V. M. Pendleton, and R. A. Johns, 1996a, 3-D seismic evidence of the effects of carbonate karst collapse on overlying clastic stratigraphy and reservoir compartmentalization: Geophysics, **61**, 1336–1350.

Hardage, B. A., D. L. Carr, D. E. Lancaster, J. L. Simmons Jr, D. S. Hamilton, R. Y. Elphick, K. L. Oliver, and R. A. Johns, 1996b, 3-D seismic imaging and seismic attribute analysis of genetic sequences deposited in low-accommodation conditions: Geophysics, **61**, 1351–1362.

Kazemeini, S. H., C. Juhlin, and S. Fomel, 2010, Monitoring CO_2 response on surface seismic data; a rock physics and seismic modeling feasibility study at the CO_2 sequestration site, Ketzin, Germany: Journal of Applied Geophysics, **71**, 109–124.

Levy, S., and D. W. Oldenburg, 1987, Automatic phase correction of common-midpoint stacked data: Geophysics, **52**, 51–59.

Liu, G., S. Fomel, and X. Chen, 2011a, Stacking angle-domain common-image gathers for normalization of illumination: Geophysical Prospecting, **59**, 244–255.

———, 2011b, Time-frequency analysis of seismic data using local attributes: Geophysics, **76**, P23–P34.

Liu, G., S. Fomel, L. Jin, and X. Chen, 2009, Stacking seismic data using local correlation: Geophysics, **74**, V43–V48.

Mendel, J. M., 1991, Tutorial on higher-order statistics (spectra) in signal processing and system theory: Proc. IEEE, **79**, 278–305.

Pollastro, R. M., D. M. Jarvie, R. J. Hill, and C. W. Adams, 2007, Geologic framework of the Mississipian Barnett Shale, Barnett-Paleozoic total petroleum system, Bend-arch–Fort Worth Basin, Texas: AAPG Bulletin, **91 (4)**, 405–436.

Robinson, E. A., and S. Treitel, 2000, Geophysical signal analysis: Society Of Explo-

ration Geophysicists.

Schoenberger, M., 1974, Resolution comparison of minimum-phase and zero-phase signals: Geophysics, **39**, 826–833.

Van der Baan, M., 2008, Time-varying wavelet estimation and deconvolution using kurtosis maximization: Geophysics, **73**, V11–V18.

Van der Baan, M., and S. Fomel, 2009, Nonstationary phase estimation using regularized local kurtosis maximization: Geophysics, **74**, A75–A80.

Van der Baan, M., S. Fomel, and M. Perz, 2010a, Nonstationary phase estimation: A tool for seismic interpretation?: The Leading Edge, **29**, 1020–1026.

Van der Baan, M., M. Perz, and S. Fomel, 2010b, Nonstationary phase estimation for analysis of wavelet character, *in* 72nd Conference and Exhibition: EAGE, D020.

Walden, A. T., and J. W. J. Hosken, 1985, An investigation of the spectral properties of primary reflection coefficients: Geophys. Prospect., **33**, 400–435.

———, 1986, The nature of the non-gaussianity of primary reflection coefficients and its significance for deconvolution: Geophys. Prospect, **34**, 1038–1066.

White, R. E., 1988, Maximum kurtosis phase correction: Geophysical Journal, **95**, 371–389.

Wiggins, R., 1978, Minimum entropy deconvolution: Geoexploration, **16**, 21–35.

Xu, Y., P. Thore, and S. Duchenne, 2012, The reliability of the kurtosis-based wavelet estimation, *in* SEG Technical Program Expanded Abstracts 2012: Society of Exploration Geophysicists.

Zeng, H., and M. M. Backus, 2005, Interpretive advantages of 90°-phase wavelets. Part 1: Modeling: Geophysics, **70**, C7–C15.

Zhang, R., X. Song, S. Fomel, M. K. Sen, and S. Srinivasan, 2013, Time-lapse seismic data registration and inversion for CO_2, sequestration study at Cranfield: Geophysics, **78**, B329–B338.